

Atmospheric Clock Transfer Based on Femtosecond Frequency Combs

Lingze Duan and Ravi P. Gollapalli
The University of Alabama in Huntsville
USA

1. Introduction

Precise timing and frequency synchronization has become ubiquitously needed as the world enters the age of global connectivity. Today's communication and computer networks are running under the regulation of synchronized time bases to ensure efficient data routing and information transfer. As the carrier frequencies of these networks continue to rise to accommodate the ever-increasing data traffic, the need for high-fidelity clock distribution becomes imperative (Prucnal et al., 1986). Within the scope of basic sciences, ultra-stable timing dissemination also becomes increasingly important as more and more highly sophisticated instrument and research facilities, such as space-borne atomic clocks (Chan, 2006), long-baseline radio telescope arrays (Cliché & Shillue, 2006), and particle accelerator-based X-ray pulse sources (Altarelli, 2007), require unprecedented level of synchronization in order to explore the uncharted physical parameter regimes.

Recently, there has been a growing interest in the research of high-fidelity, remote transfer of reference clock signals using femtosecond frequency combs (Foreman et al., 2007; Kim et al., 2008). The rationale behind the idea is that frequency combs can conveniently acquire their timing stability from optical atomic clocks, the next generation timing standard, and transfer the stability of an atomic clock at a fixed frequency onto a number of spectral lines (as many as $\sim 10^5$ - 10^6) over a broad spectrum in *both* optical and microwave frequency regions. These features give frequency combs enormous advantage as a carrier of timing and frequency references over conventional single-frequency lasers, which can only transfer a single channel of clock signal in *either* the optical or the microwave frequency region.

Over the last two years, we have proposed and experimentally demonstrated atmospheric remote clock transfer based on a femtosecond frequency comb (Alatawi et al. 2009; Gollapalli & Duan, 2010). It is a complementary scheme to the previously studied fiber-optic remote delivery of frequency combs (Holman et al., 2004). Compared to fiber-optic delivery, transferring frequency combs through the atmosphere does not rely on the existence of a wired system and hence reduces the cost while offering a much better flexibility. It is particularly desirable for timing synchronization between moving transmitters and receivers, such as motor vehicles, ships, airplanes and satellites, and it is the preferred scheme when a close-range, short-term transfer link is needed. Moreover, future space-terrestrial network will need high-fidelity optical up-and-down links to synchronize space-borne atomic clocks with ground-based atomic clocks (Chan, 2006). Pulse laser-based timing synchronization offers a viable solution to the establishment of such links.

Photodetection plays a key role in laser-based synchronization systems because it converts the timing signals stored in the photons into electronic form so the information can be read by the instruments under synchronization. Photodetectors are essential components in the study of laser remote clock transfer. Their unique impacts on the characterization of atmospheric frequency comb transmission are two-fold. First, the “square-law” nature of photodetectors leads to two completely different system configurations for the transfer of timing signals in the radio/microwave frequency (RF) range and in the optical frequency range, i.e. RF heterodyne and optical heterodyne. Second, atmospheric optical effects such as beam wander and speckle induce strong amplitude noise in the heterodyne signal, which enters the phase noise characterization as a limiting noise source due to the power-to-phase coupling effect in photodetectors.

In this chapter, we will give an overview of the recent progress in our study of atmospheric clock transfer based on femtosecond frequency combs. We shall first review the concept and the basic characteristics of femtosecond frequency combs. Then we will discuss the technical specifics associated with the atmospheric clock transfer experiment, especially the roles of photodetectors in different heterodyne schemes and the impact of power-to-phase coupling in the phase noise measurement. The two sections following that will be devoted to the experimental results, first with the clock signal in the RF range ($\sim 10^9$ Hz) and then with the clock in the optical frequency range ($\sim 10^{14}$ Hz). We shall compare our results with similar experiments based on cw (continuous-wave) lasers and summarize at the end.

2. Femtosecond frequency combs

2.1 The concept of frequency combs

The concept of optical frequency combs was initially introduced as a way to bring frequency metrology into the optical region (Udem et al., 2002). The advance in precision spectroscopy and optical sensing requires that optical frequencies, which fall in the range of 100–1000 terahertz (THz) for the IR-Visible-UV band, be measured with accuracies comparable to microwaves. Such a level of accuracy can only be achieved with a metrological link that can directly reference optical frequencies to Cs atomic clocks, which operate at about 9.2 GHz (Hall & Ye, 2003). The emergence of solid-state femtosecond lasers in the late 1990s allowed this concept to be experimentally realized (Jones et al., 2000). In essence, a femtosecond frequency comb is simply a frequency-stabilized ultrafast laser (Holzwarth et al., 2000). Such lasers are able to produce optical pulses as short as a few femtoseconds (10^{-15} s) at very fast pulse repetition rates (~ 0.1 – 10 GHz). The result is a pulse train with a constant pulse interval, as shown in Fig. 1 (a). The spectrum of such a pulse train consists of a series of equally spaced spectral lines (often referred to as comb lines), spanning across an extremely broad spectral range owing to the ultra-short temporal profiles of the femtosecond pulses.

A conceptual illustration of such a supercontinuum spectrum is depicted in Fig. 1 (b). With proper electronic control, the pulse repetition rate (i.e. the spacing of the comb lines) and the carrier-envelope offset (CEO) frequency (i.e. the offset frequency of the comb when it is extended to zero), both in the microwave frequency range, can be stabilized against an atomic reference, such as a Cs clock (Udem et al., 2001). This establishes a grid of well-defined spectral markers through the simple relation of $f_m = f_{CEO} + mf_R$, where f_R and

f_{CEO} are the repetition rate and the CEO frequency, respectively, and m is the index number of the comb line in concern. Unknown spectral features within the span of the supercontinuum can be compared with these comb lines through interference and their exact frequencies can be determined with kilohertz-level resolutions or even better (Fortier et al., 2006).

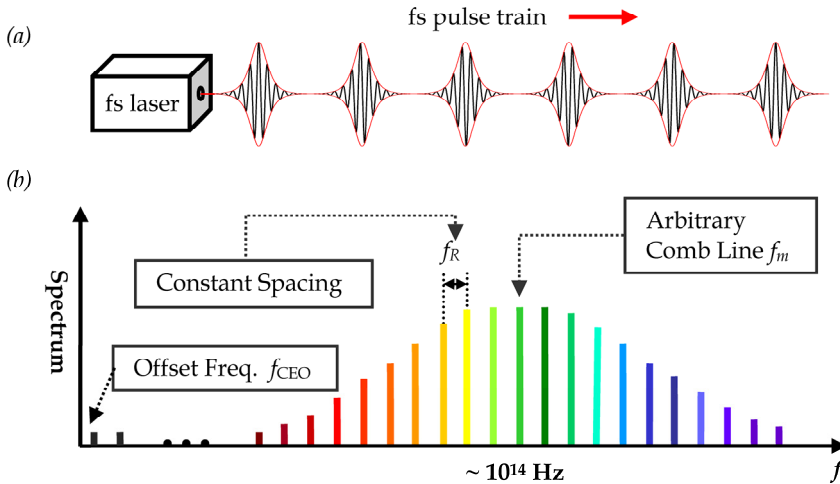


Fig. 1. Concept of femtosecond frequency combs. (a) time-domain picture – a femtosecond pulse train with a fixed pulse interval; (b) frequency-domain picture – a supercontinuum that consists of a series of equally-spaced spectral lines. The frequency of an arbitrary comb line has two degrees of freedom defined by $f_m = f_{CEO} + mf_R$. Locking f_R and f_{CEO} , or any two independent combinations of them to atomic clocks will transfer the frequency accuracy of the clocks onto the entire spectrum.

2.2 Key characteristics of frequency combs

Once stabilized, a femtosecond frequency comb offers some unique features unattainable with other types of laser systems. For example, it combines a supercontinuum spectrum, often spanning across more than an octave, with ultrahigh spectral precision for individual comb lines, which in the past could only be achieved with cw lasers operating at a single frequency. Sub-hertz linewidth across the entire comb spectrum (e.g. 580–1080 nm) has been reported (Bartels et al., 2004). This feature allows a frequency comb to combine the accuracy of a single-frequency laser and the flexibility of a supercontinuum source, and hence leads to a wide range of applications such as trace-molecule detection (Thorpe et al., 2006), precise ranging (Ye, 2004) and extrasolar planet search (Li et al., 2008).

Another interesting feature for a femtosecond frequency comb is that, besides the precisely defined grid of *optical* frequencies, the comb also carries a grid of highly stable *microwave* frequencies stemming from the constant pulse repetition rate. These frequency references can be easily accessed via photodetection. A photodetector essentially converts the ultra-

stable timing of the pulses into a series of discrete spectral lines consisting of the harmonics of the repetition rate. A femtosecond frequency comb hence can be treated as a carrier of timing/frequency references, or “clocks”. But unlike conventional clock carriers, such as cw lasers or RF communication channels, which can only carry one single frequency at a time, a frequency comb simultaneously carries multiple ($\sim 10^5$ - 10^6 in some cases) clock signals in both microwave and optical frequency ranges. Such a capability offers femtosecond frequency combs unprecedented versatility in remote clock transfer (Foreman et al., 2007), which we shall focus on in the rest of the chapter.

2.3 Frequency comb-based clock transfer

One important recent development in the application of femtosecond frequency combs is the demonstration of comb-based high-fidelity remote clock transfer through optical fibres (Holman et al., 2004; Holman et al., 2005; Foreman et al., 2007; Kim et al., 2008). In the microwave frequency range, a fractional frequency instability of $<9 \times 10^{-15}$ for a 1-s averaging time has been achieved through a 6.9-km installed fibre link with the help of active noise cancellation (Holman et al., 2005). In the optical frequency range, two lasers connected by a 300-m fibre link have been synchronized for 12 hours with a relative timing instability of 9×10^{-21} (Kim et al., 2008). These results are comparable to or exceeding the performance of the conventional techniques, which use a modulated cw laser to transfer a single microwave clock and rely on an ultra-stable single-frequency laser to deliver an optical frequency reference (Foreman et al., 2007). Thus, femtosecond frequency combs are not only efficient and versatile, but effective as well in terms of remote clock delivery via fibre networks.

The success of comb-based clock transfer in fibre logically leads to the question about free-space clock distribution using femtosecond lasers. This will not be a trivial extension from the work done in fibre because the transmission medium now becomes air, which is much more dynamic than glass. New phenomena are expected to dominate and new strategies are needed. In fact, the research on optical pulse propagation in the air dates back to the 1970s. In the context of optical communications, various models of pulse propagation in turbulent random media have been studied (Su & Plonus, 1971; Liu et al., 1974; Hong et al., 1977; Young et al., 1998). Today, femtosecond transmission in the atmosphere continues to attract much attention because of its potential applications in remote sensing and Light Detection and Ranging (LIDAR). Topics in this area that attract major research interest include nonlinear effects, ionization, atmosphere turbulence, and their impact on pulse propagation (Akozbeq et al., 2000; Mlejnek et al., 1999; Sprangle et al., 2002; Rodriguez et al., 2004). However, most of the previous work on atmospheric propagation of femtosecond pulses focuses on the interactions between air and individual pulses. Little attention has been given to the propagation of a pulse train as a whole in the atmosphere, especially in terms of the precision degradation of its Fourier frequencies. The work described in the following aims to address this important aspect through experimental characterizations.

3. Atmospheric remote transfer of frequency combs

Before we begin the discussion about specific experiments, it is necessary to review several general technical aspects associated with these experiments so that readers can gain a better understanding of the physical background behind some of the techniques involved.

3.1 Noise sources in atmospheric transmission

The key question we seek to answer through the current research is: How much extra noise will be added to the clock signals as the femtosecond pulse train propagates through the air? To answer the question, we must first take a look at the potential noise sources in the atmosphere. Two major mechanisms can cause the degradation of clock precision in the air - temporal fluctuation of the refractive index and scattering (Ishimaru, 1978). Air turbulence creates random density fluctuations, resulting in a time-dependent average refractive index over the path of the laser beam, which leads to variation of pulse arrival time. On the other hand, density inhomogeneities in the air, along with scattering particles such as aerosols, may cause pulses being randomly scattered, as shown in Fig. 2. This may lead to pulse distortion and dephasing, which degrade the timing precision of the original pulse train and broaden the comb lines.

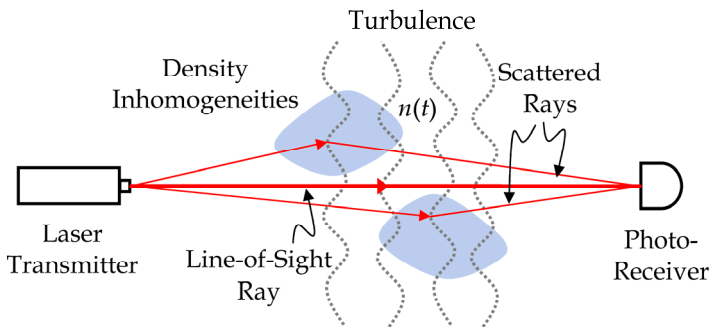


Fig. 2. The effects of index fluctuation and scattering on atmospheric optical transmission.

For ground-level short-distance (e.g. < 1 km) transmission links, one can assume clear air and weak turbulence (Andrews & Phillips, 2005). Under such conditions, it has been shown that scattering plays a far less important role in affecting the pulse arrival time compared to pulse wandering due to index fluctuation (Liu & Yeh, 1980). The transmission distance in our experiments is about 60 m, and we usually avoid taking measurement under extreme weather conditions such as rainy, foggy or highly windy days. Therefore, it is justified to ignore scattering in our research and focus only on the index fluctuation in line-of-sight beam propagation. In addition, it should be pointed out here that turbulence and scattering also cause beam pointing fluctuation and speckle, which affect the received pulse amplitude as well. Special care must be taken in the design of the optical system to minimize the impact of these effects. Specific discussions about some of these measures will be made in Section 3.4.

3.2 Excess phase noise and frequency instability

For an infinite periodical pulse train, the temporal variation of the pulse arrival time due to atmospheric transmission broadens the spectral lines in the Fourier domain, introducing excess phase noise to the initially highly precise grid of Fourier frequencies. The phase noise spectrum can be determined via a heterodyne process, which compares the transmitted pulse train with its copy from a reference path that induces negligible phase noise. By

spectrally analyzing the heterodyne signal, we can measure the power-spectral density (PSD) of the phase-noise generated sidebands, $S_\varphi(f)$, representing the mean-squared phase fluctuation at a Fourier frequency f away from the centre frequency with a 1-Hz bandwidth of measurement (Foreman et al., 2007),

$$S_\varphi(f) = [\delta\varphi(f)]^2 \quad (\text{rad}^2/\text{Hz}) \quad (1)$$

Sometimes it is more convenient to characterize phase noise in terms of pulse timing jitter, which is defined as

$$\delta T(f) = \frac{\delta\varphi(f)}{2\pi\nu_0} \quad (\text{s}/\sqrt{\text{Hz}}), \quad (2)$$

where ν_0 is the centre frequency. Integrating the spectral density of the timing jitter over the measurement bandwidth, from f_l to f_h , leads to the total rms timing jitter of the pulses

$$T_{rms} = \sqrt{\int_{f_l}^{f_h} [\delta T(f)]^2 df} \quad (\text{s}). \quad (3)$$

The spectrum of the excess phase noise or timing jitter essentially characterizes the short-term (usually < 1 s) stability of the clock transmission link.

The second aspect in the characterization of clock stability is how much the time-averaged frequency varies over different lengths of the averaging period. It is usually used to describe the stability of a frequency signal over relatively longer term, e.g. > 1 s. Experimentally, this is done by measuring the Allan deviation of the frequency signal over an averaging time τ , which is defined as

$$\sigma_y(\tau) = \left\langle \frac{1}{2} [\bar{y}(t+\tau) - \bar{y}(t)]^2 \right\rangle^{1/2}, \quad (4)$$

where $\bar{y}(t)$ is the time average of the instantaneous fractional frequency deviation from the centre frequency (Allan, 1966).

The phase noise/timing jitter spectrum and the Allan deviation characterize clock instability from different perspectives. They are the main quantities we seek to determine through our experiments.

3.3 RF heterodyne vs. optical heterodyne

The heterodyne technique has long been used in RF technologies to shift information signals from one frequency channel to another (Nahin, 2001). In the current research, in order to study the phase noise sidebands due to pulse propagating in the atmosphere, we need to shift the noise sidebands to lower frequencies where a fast Fourier transform (FFT) analyzer can effectively resolve the noise spectrum. Conceptually, this can be easily done by beating the noisy signal with a noise-free local reference, which has a frequency identical or close to the centre frequency of the noisy signal. At the output of the heterodyne mixer, the noise sidebands are shifted to both the sum and the difference frequencies. With a low-pass filter,

we can select the downshifted bands at the difference frequency. In the case the difference frequency is zero, i.e., the noisy signal and the reference have the same centre frequency, the noise sidebands are shifted to the base band, and the lower sideband is folded into the positive side by the FFT. Fig. 3 (a) & (b) give a conceptual sketch of this heterodyne process. The reference signal can be obtained by splitting a portion of the original clock at the output of the source. This also greatly reduces the impact of the source noise to the measurement as the source noise is common-mode and hence is cancelled at the difference frequency.

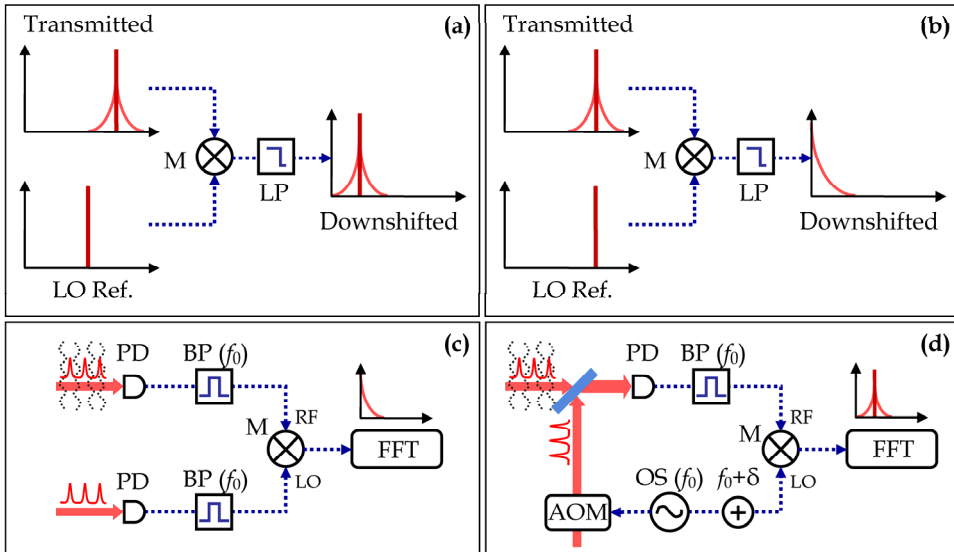


Fig. 3. Concept of heterodyne noise measurement with (a) different centre frequencies and (b) same centre frequency. Configurations of (c) RF heterodyne and (d) optical heterodyne. BP, bandpass filter; LP, lowpass filter; M, mixer; OS, oscillator; PD, photodiode.

In practice, two different heterodyne configurations are used for the two clock frequency ranges, namely RF heterodyne and optical heterodyne. The necessity originates from the use of square-law detectors. Photodetectors, such as photodiodes, are known to be square-law detectors. They cannot directly respond to the optical field due to the short optical cycles (\sim fs). Instead, they respond to the quantized excitations of the optical field, i.e. photons. This is equivalent to finding the time-averaged intensity, which is proportional to the “square” of the optical field (Davis, 1996). As a result, the optical cycle is averaged out and the detector can only probe the slow variation of the field envelope. However, a square-law detector can respond to the beat frequency of two optical fields with a small frequency difference when they are incident on the detector simultaneously. To understand this effect, we shall assume optical waves A and B with a slight frequency offset $\Delta\omega$ superpose on a photodetector. The total field can be written as

$$\vec{E} = \vec{A} \cos \omega t + \vec{B} \cos(\omega + \Delta\omega)t. \tag{5}$$

The detector responds to the time-averaged intensity I , which can be expressed as

$$I \equiv \varepsilon_0 c \langle \vec{E} \cdot \vec{E} \rangle = \varepsilon_0 c \left(\frac{A^2}{2} + \frac{B^2}{2} + \vec{A} \cdot \vec{B} \cos \Delta \omega t \right), \quad (6)$$

where $\langle \rangle$ indicates time-average, and ε_0 and c are free-space permittivity and speed of light, respectively. The last term on the right hand side is the interference term, which oscillates at the beat frequency. It can be detected by the photodetector as long as it falls within the detector's bandwidth. From this point of view, a photodetector can be used as a heterodyne mixer to generate an electric oscillation at the difference frequency of the two optical fields. This feature of photodetectors becomes the basis of optical heterodyne.

In Fig. 3 (c) and (d), we use our experiments as examples to illustrate the concepts of RF heterodyne and optical heterodyne. In the RF heterodyne, two identical photodetectors convert the femtosecond pulse trains from both the transmitted arm and the reference arm into a series of electric oscillations at the harmonics of the pulse repetition rate. One of these frequency components is selected by bandpass filters in both arms as the clock under study. The transmitted clock with excess phase noise is then mixed with the reference clock at a double-balanced mixer to generate the heterodyne beat signal, which is spectrally analyzed by an FFT analyzer to give the noise spectrum. In the optical heterodyne, the pulse trains from the two arms are first mixed on a photodetector. The reference beam gains a slight frequency shift f_0 at an acousto-optical modulator (AOM). As a result, the photodetector produces a beat signal at f_0 . This beat signal is further downshifted via RF heterodyne to make it accessible by the FFT analyzer. As we shall discuss in Section 5, for optical clock transfer, it is more convenient to keep the final beat signal away from the base band so that the full line shape can be seen.

One unique feature of optical heterodyne with femtosecond frequency combs is the process of multiheterodyne. When two frequency combs are mixed on a photodetector, each pair of corresponding comb lines from the two arms produces a beat signal. The total heterodyne signal is a coherent superposition of all these beat notes from individual comb lines. The analysis of multiheterodyne of frequency combs is out of the scope of this chapter. In-depth discussions can be found elsewhere (Gollapalli & Duan, 2011).

3.4 Power-to-phase coupling in photodiodes

When a photodiode is directly used to extract microwave signals from a modulated optical signal, additional phase noise is generated in the spectra of the microwave signals due to power-to-phase conversion in photodiodes (Tulchinsky & Williams, 2005). When the optical signal is an ultrafast pulse train, this excess phase noise can be found at the harmonics of the pulse repetition rate, causing extra fluctuations to the microwave clock signals extracted from the pulse train (Ivanov et al., 2003). The exact physical mechanisms of the power-to-phase conversion in photodiodes are not completely clear. One likely cause is the saturation of photodetectors (Liu et al., 1999). When the average power of the optical signal reaches certain level, space-charge build-up in the depletion region of the photodiode reduces the electric field in the depletion region, leading to a reduction of the velocity of photogenerated carriers and hence a phase delay in the photocurrent. Clear correlations between the arrival times of the photocurrent pulses and the incident optical power have been observed experimentally (Bartels et al., 2005).

The presence of power-to-phase coupling in photodetectors results in a detector-induced excess phase noise, which, in the case of microwave clock transfer, could mask the excess phase noise due to transmission. Two unique factors affecting the quality of atmospheric laser communication are beam wander and speckle (Andrews & Phillips, 2005). Both effects have been visually observed in our experiment. One of their consequences is optical power fluctuation on the photodetector. The excess phase noise due to power-to-phase coupling can make a significant contribution to the total measured phase noise. In order to evaluate the impact of this detector-induced phase noise, we use a microwave power detector to monitor the power of the extracted clock signal and measure the correlation between the detected phase noise and the clock power (see Section 4.2 and Fig. 5 for description of the experimental setup). Under linear operation, the power of the recovered clock scales as the square of the optical power received by the photodiode. However, the fluctuation of the clock power can be treated as linearly proportional to the fluctuation of the optical power near the average power level. Therefore, the correlation between the phase noise and the fluctuation of the clock power actually reflects the correlation between the phase noise and the optical power fluctuation. Correlation is determined by recording the coherence function between the measured phase noise and clock power during each data run. Here “coherence” is defined as

$$C_{yx}(f) = \frac{\Phi_{yx}(f)}{\sqrt{\Phi_{yy}(f) \cdot \Phi_{xx}(f)}}, \quad (7)$$

where $\Phi_{xx}(f)$ and $\Phi_{yy}(f)$ are the power spectral densities of time series x and y (as functions of Fourier frequency f), and $\Phi_{yx}(f)$ is the cross-power spectral density between the two series. By definition, the coherence function ranges between 0 and 1.

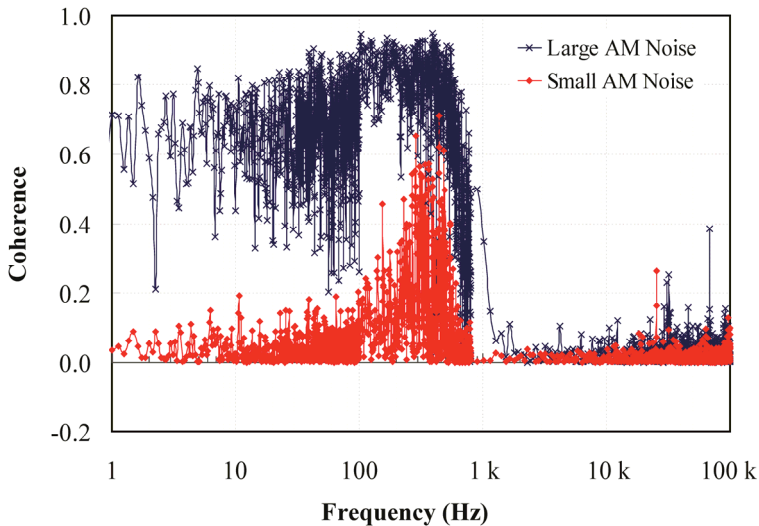


Fig. 4. The correlation (in terms of coherence function) between the measured phase and clock power indicates the impact of power-to-phase coupling in the photodiode.

Fig. 4 shows the measured phase-power coherence under two experimental configurations. The blue cross trace is obtained with a fibre-coupled photodiode and a fibre collimator receiving the transmitted laser beam. Since the coupling efficiency of the collimator critically depends on beam pointing and transverse intensity distribution of the incident beam, the power coupled to the detector is very sensitive to beam wander and speckle. As a result, a significant amount of phase noise is generated by the photodiode due to power-to-phase coupling. This is indicated by the coherence values close to 1 below 1 kHz. Apparently, such a system configuration would not allow us to effectively evaluate the transmission-induced phase noise because of the overwhelming contribution from the detector. Therefore, in the second configuration, we use large-diameter optics (e.g. 2 inch) in the receiving system and focus the beam directly onto the photodiode with the size of the focus much smaller than the active area of the detector. Such a configuration keeps the receiving system insensitive to the beam pointing drift and the transverse beam-profile variation. As the red diamond trace shows, the coherence function is close to zero over a wide frequency range, indicating little phase-power correlation at these frequencies. A moderate peak of coherence (~ 0.5) at a few hundred hertz can be attributed to temporal fluctuation of the irradiance due to scintillation of the laser beam (Andrews & Phillips, 2005). But its impact to the phase noise measurement is very limited because the noise spectrum rolls off quickly at such high frequencies.

4. Atmospheric transfer of microwave timing signals

As pointed out in Section 2, the ultrastable pulsing rate of a femtosecond frequency comb can be used as a clock signal. The repetition rates of most common femtosecond lasers range from tens of MHz to 1 GHz or so. Their harmonics, however, can be much higher. A femtosecond pulse train inherently carries all these harmonics simultaneously, and their retrieval as timing references is only limited by the bandwidths of the photodetectors used.

4.1 A rooftop transmission link

In order to study frequency comb-based atmospheric clock transfer, we established an outdoor laser transmission link. The link is located on the roof of our laboratory building on

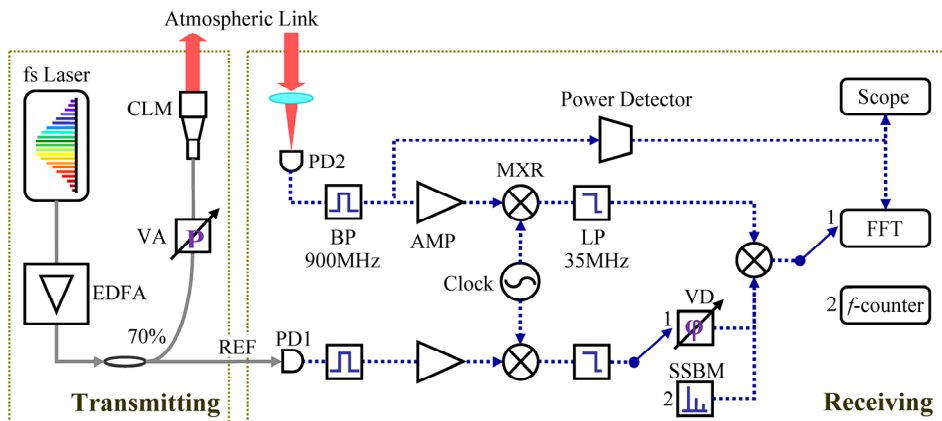


Fig. 5. Schematic layout of the test system for atmospheric microwave timing transfer. AMP, RF amplifiers; BP, band-pass filters; LP, low-pass filters; MXR, double-balanced mixers; PD, photodiodes; VA, variable attenuator; and VD, variable delay.

the campus of the University of Alabama in Huntsville. The four-floor building has an observation platform about 20 meters above the ground. There is no high-rise building or other tall structure nearby to create local turbulence. A sturdy steel tripod is anchored on the platform to house a metal beam reflector (a 2-inch gold mirror). The laser beam is launched from a nearby astronomical observatory into the open air and the reflector sends the beam back to the observatory, where all the signal processing and measurement takes place. The round-trip propagation distance is about 60 m.

4.2 Experimental setup

Fig. 5 shows the schematic of the experimental setup for microwave timing transfer. The system is divided into transmitting and receiving subsystems. In the transmitting part, a femtosecond fiber laser (Precision Photonics FFL-1560) generates a train of 150-fs pulses centered at 1560 nm, with a 90-MHz repetition rate and a 4-mW average power. An erbium doped fiber amplifier (EDFA) boosts the average power to 100 mW. A 70:30 broadband fiber coupler directs the majority of this power into a fiber collimator, which launches a 7 mm-diameter beam into the atmospheric transmission link. A fiber-coupled variable attenuator is inserted before the collimator as a power regulator to provide precise control over the total optical power reaching the receiving photodiode.

In the receiving subsystem, the transmitted beam is tightly focused onto a high-speed photodiode, which recovers the repetition frequency of the femtosecond laser as well as its harmonics. The 10th harmonic at 900 MHz is chosen as the microwave clock under test and is selected by a bandpass filter. To further reject the side modes, a local clock is used to beat the 900 MHz signal down to 35 MHz, where sharp low-pass filters can effectively remove all the remaining harmonics. Meanwhile, a reference clock signal is obtained by coupling a small portion of the EDFA output directly into the receiving subsystem via optical fiber (the REF path in Fig. 1) and then using a microwave circuit similar to the transmitted clock. The resulted frequency signal serves two sets of measurement. In the phase noise measurement, the reference clock passes through an adjustable delay line to gain a proper phase before it beats the transmitted clock in quadrature at a double-balanced mixer. The generated phase signal is frequency analyzed by a Fast Fourier Transform (FFT) analyzer (SRS SR785) and timing jitter spectral density can be calculated from the phase noise spectrum. In frequency stability measurement, the reference clock is frequency-shifted by 500 kHz through a single-sideband modulator (SSBM) and then mixed with the transmitted clock. This leads to a 500-kHz beat note, which is then measured with a frequency counter (SRS SR620) to determine its stability. It should be noted here that, although the repetition rate of the femtosecond laser is not stabilized in the test, the noise from the laser and the EDFA does not affect the measurement because it is common mode in the above heterodyne scheme. This ensures correct characterization of the excess clock instability due to the atmospheric propagation.

4.3 Laboratory test

In order to verify that the sensitivity of our experimental system is sufficient to measure the excess phase noise due to small index fluctuation in the air, we have first conducted a proof-of-principle test inside the lab, where the airflow can be better controlled. The main source of index fluctuation in this case is the air-conditioning (AC) airflow, predominantly moving downward across the laser beam. To verify the coincidence between the AC airflow and the

phase noise, we fix the total length of the transmission link (~ 10 m) but change the effective beam path exposed in the AC airflow by inserting rigid plastic tubes (2.5 cm inner diameter) in the beam path. We find that the tubes can effectively control the measured phase noise. In addition, we have also made measurement with the AC system off and found the noise to be much lower. These facts confirm the effectiveness of our measurement system (Alatawi et al. 2009). Fig. 6 (a) shows the spectra of the transmission-induced timing jitter at four effective beam path lengths over a Fourier frequency range of $10^{-2} - 10^5$ Hz, along with the system noise (measured with a negligible beam path in the air). The system noise, mainly attributed to the RF amplifiers and the mixers, has a $1/f$ power frequency dependence below 1 kHz,

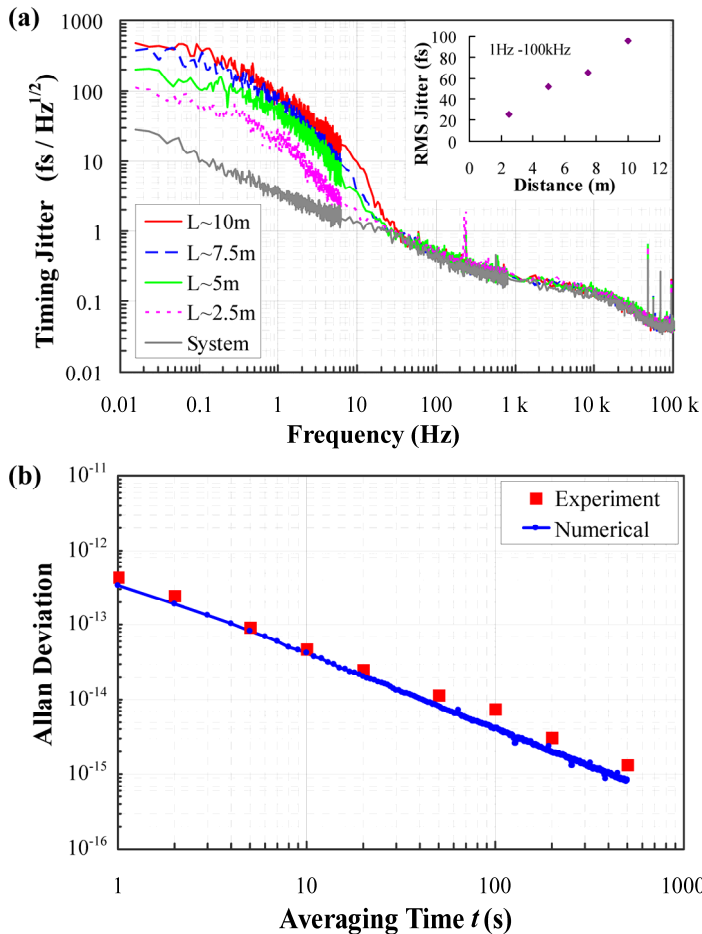


Fig. 6. (a) Spectral density of the excess timing jitter for four effective transmission distances, along with the system noise floor; inset: the total rms jitter integrated from 1 Hz to 100 kHz vs. effective beam path length in AC airflow. (b) The measured Allan deviation with a 10-m effective beam path and the numerical estimation based on the phase noise measurement.

indicating a Flicker phase noise that commonly exists in RF amplifiers within this frequency range (Halford et al., 1968). As the frequency increases, the noise floor gradually shifts toward white noise. The transmission-induced phase noise only becomes appreciably above the system noise below a few tens of hertz. As the Fourier frequency goes down, the power law of the noise gradually changes and eventually shows a trend toward f^0 below 0.1 Hz. Such behaviour is markedly different from what has been observed in fibre (Holman et al., 2005). To further verify the dependence of the excess phase noise on the AC airflow, we have calculated the rms timing jitter at different effective beam path lengths by integrating the timing jitter spectra in Fig. 6 (a) from 1 Hz to 100 kHz. For effective path lengths of 2.5, 5, 7.5, and 10 m, the total rms jitters are 37.5, 58.9, 71.2, and 99.0 fs, respectively, and the total rms jitter caused by the system noise is 27.5 fs. Fig. 6 (a) inset shows a near linear relation between the total *actual* rms timing jitter (system noise excluded) and the beam path length exposed in the airflow, confirming a direct correlation between airflow and phase noise.

The long-term transfer instability for 10-m effective beam path is evaluated by measuring the Allan deviation σ_y of the beat note frequency at a set of different averaging times. Fig. 6 (b) shows a typical set of experimental data, along with a set of numerical data based on the timing jitter measurement shown in Fig. 6 (a). The calculation uses the relation between the spectral density of phase noise and the Allan deviation (Rutman & Walls, 1991)

$$\sigma_y^2(\tau) = 2 \int_0^{f_h} S_y(f) \frac{\sin^4(\pi\tau f)}{(\pi\tau f)^2} df, \quad (8)$$

where f_h is the bandwidth of the system low-pass filter. The excellent agreement between the two sets of data demonstrates the effectiveness of our measurement in assessing the excess clock fluctuation caused by atmospheric transmission.

4.4 Outdoor test

Once the measurement scheme passes the lab test, we apply it to the rooftop transmission link. Excess phase noise has been measured at different times of a day and under various weather conditions (except rainy days). The corresponding timing jitter is then calculated from the phase noise spectrum using (2). Fig. 7 (a) shows several typical traces of the jitter spectral density, along with the system noise baseline. The excess timing jitter is above the baseline only at frequencies below several hundred hertz. The magnitude and frequency dependence of the jitter spectra are strongly affected by the weather conditions, especially the wind speed, leading to a group of different spectral traces under otherwise similar conditions. The system baseline is mainly attributed to the RF amplifiers in the receiving system, and the noise spikes around 10-200 Hz are believed to be due to electric interference caused by the utility circuitry in the observatory. Fig. 7 (b) shows the rms jitter integrated from 1 Hz to the frequency in concern for all five traces in (a). Clearly, most contributions to the rms jitter come from noise below 100 Hz, indicating the dominance of slow phase modulations. The total rms jitters integrated from 1 Hz to 100 kHz range from several hundred femtoseconds to about two picoseconds. The system noise proves to have a negligible effect in the measurement as evident from its sub-100-fs effective rms jitter.

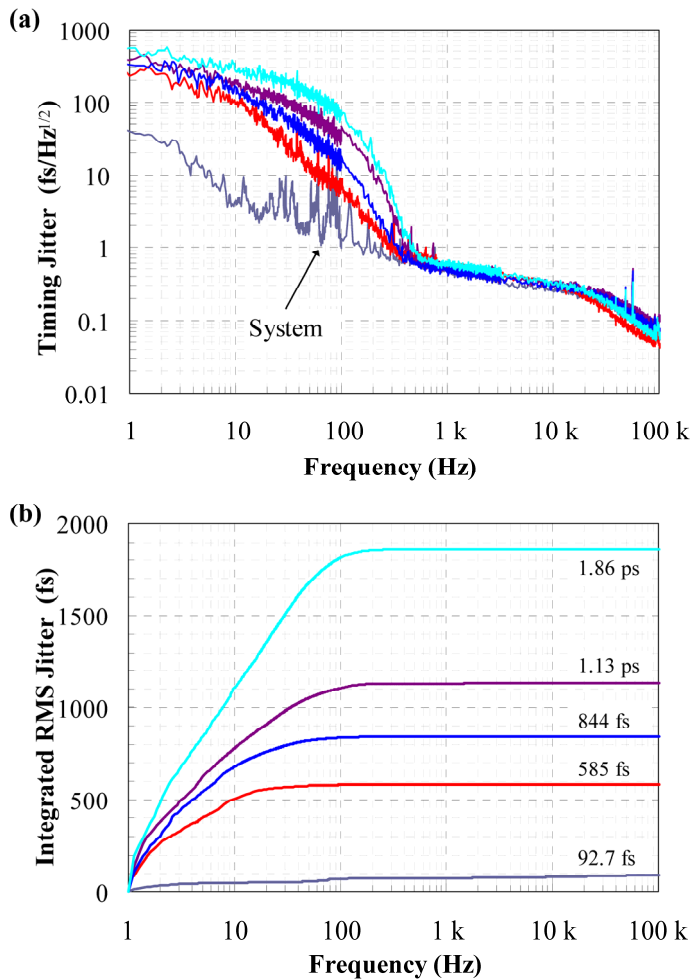


Fig. 7. Transmission-induced pulse timing jitter after a femtosecond frequency comb propagates 60 m through open atmosphere under various weather conditions. (a) Typical timing jitter spectra along with the system noise. (b) The integrated rms jitters for the five spectra in (a). The numbers are the RMS jitters integrated from 1 Hz to 100 kHz.

The result of the Allan deviation measurement is shown in Fig. 8, which also includes the trace from the 10-m indoor test for the purpose of reference. The fractional frequency stability after 60-m atmospheric transmission is in the order of a few parts per trillion at a 1-s averaging time τ . This is comparable to the frequency stability of most commercial atomic timing references, such as Cs or Rb clocks. At longer averaging times, the Allan deviation falls at a rate close to τ^{-1} , indicating white phase fluctuations (IEEE, 1983). This is different from fiber optic transmission, where the Allan deviation falls at $\tau^{-1/2}$ (Holman et al., 2004). It should also be noted that most atomic timing references also have a $\tau^{-1/2}$ behaviour. As a result, transferring

a master microwave timing reference through free space becomes more advantageous than maintaining a less-precise local clock when the clock signal is averaged over longer time.

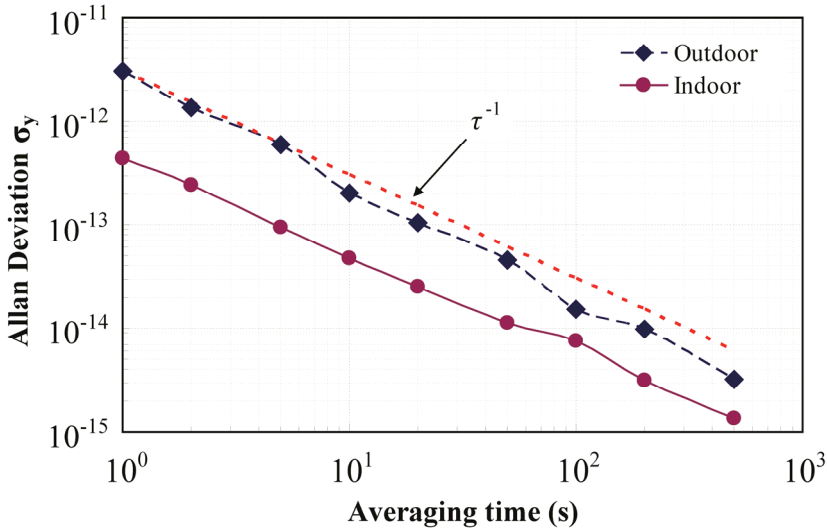


Fig. 8. A typical set of measured Allan deviation (diamond) of the 900 MHz clock signal after 60-m atmospheric propagation shows an approximate τ^{-1} dependence over the averaging time τ . The baseline data (circle) are obtained under indoor conditions with a much lower wind speed.

4.5 Discussion

The propagation of an optical pulse train through an atmospheric communication channel is susceptible to the refractive-index fluctuation caused by clear-air turbulence (Su & Plonus, 1971). From the rms timing jitter, we can derive the rms fluctuation of the group index n_g by using the relation $\Delta n_g = (c/L)\Delta T$, where c is the speed of light in vacuum, L is the total propagation distance, and ΔT represents the rms timing jitter. By using $\Delta T = 2$ ps and $L = 60$ m, we find the value of Δn_g to be 1×10^{-5} . Meanwhile, it has been shown that $\Delta n_g \approx a \cdot \Delta n$, where Δn is the fluctuation of the phase index and the proportional constant a is approximately equal to 3 in the visible and near infrared wavelength range (Ciddor, 1996; Ciddor & Hill, 1999). This leads to an estimated rms phase index fluctuation of several parts per million, which agrees with the well-known scale of such fluctuation due to clear-air turbulence (Shaik, 1988).

The measured timing transfer stability is compared with a similar rooftop experiment over a 100-m open link using the conventional carrier-modulation scheme (Sprenger et al., 2009). The fractional instability at 1 s measured in our test is several times smaller than the result presented in the reference. Moreover, their Allan deviations appear to have an averaging-time dependence close to $\tau^{-1/2}$ below 100 s, while our result is close to τ^{-1} . Such a difference in Allan deviation behaviour indicates possible difference in the underlying

mechanism of instability. In fact, as pointed out by the authors, the earlier experiment is likely limited by the stability of the frequency synthesizers, and therefore only offers an upper bound of the propagation-induced instability. This seems to be supported by the fact that the electronic timing instrument usually shows a $\tau^{-1/2}$ characteristic. Such a system-noise limitation is partly because of the low clock frequency (80 MHz) used in the earlier work. In comparison, our experiment is free from such a restriction, as shown by the baseline data, because the wide bandwidth of the femtosecond pulses allows the use of a higher harmonic of the repetition rate as the clock signal.

5. Atmospheric transfer of optical frequencies

While clock signals in the microwave frequency range can be delivered by a femtosecond frequency comb and conveniently extracted with a photodetector, it is the ability to carry many optical frequency references that makes frequency combs very attractive as a clock transfer means. This is not only because the much higher frequencies of optical clocks lead to better fractional stability, but because optical frequency references can directly benefit from the next-generation atomic clocks, which will work in the optical frequency range.

5.1 Experimental setup

In order to demonstrate the capability of a femtosecond frequency comb to transfer optical frequency references through free space, we convert our rooftop experimental setup shown in Fig. 5 into an optical heterodyne configuration. Fig. 9 shows the new schematic layout. The system is again divided into transmitting and receiving subsystems. The transmitting subsystem is similar to the one used in the microwave clock transfer tests. The receiving

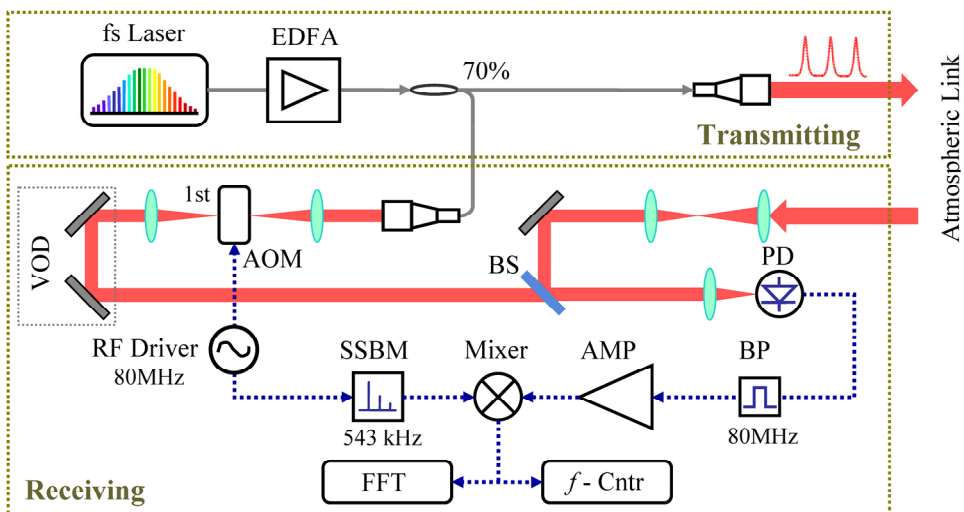


Fig. 9. Schematic layout of the experimental system for atmospheric transfer of optical frequency references. AMP, microwave amplifiers; BS, beam splitter; PD, photodiode; SSBM, single-side band modulator; and VOD, variable optical delay.

subsystem features an optical heterodyne configuration as discussed in Section 3.3. The reference beam passes through an AOM, which is driven by a RF driver at 80 MHz, and the first-order deflection is selected. Meanwhile, the beam transmitted through the atmospheric link is coupled into the receiving subsystem by a lens pair, which converts the expanded beam into a comparable size to the reference beam. The two beams are then combined into collinear propagation at a broadband beam splitter and focused onto a photodiode. A variable optical delay line in the reference arm ensures temporal overlapping of the transmitted pulses and the reference pulses. The photodiode produces an 80-MHz beat note from the two beams. The beat note is then phase-compared with a portion of the original 80-MHz driving signal at a double-balanced mixer. In order to measure the linewidth of the beat note, a small frequency shift (about 543 kHz) is added to the original 80-MHz signal through a single-sideband modulator (SSBM). The resulted 543-kHz beat signal is analyzed by an FFT analyzer for direct spectral width measurement and a frequency counter for frequency stability measurement. It should be noted here that the design of the receiving optical system has been made with the consideration of minimizing the impact of speckle and beam wander as discussed in Section 3.4.

5.2 Experimental results

The frequency transfer test was performed over the course of three months in the summer of 2010. Data have been taken under low-wind conditions with the wind speed below 2 m/s. Strong phase fluctuations in the multiheterodyne signal have been observed as pictured in Fig. 10 (a) inset. Time-domain phase traces like Fig. 10 (a) inset are taken by mixing the 80-MHz beat note from the photodiode directly with the original 80-MHz AOM driving signal without the SSBM. The fast oscillation of the beat note phase indicates a phase modulation index much greater than 2π . In order to examine the Fourier spectrum of the beat note, we add a small frequency offset of 543 kHz using the SSBM onto the 80-MHz reference from the AOM driver so that the beat signals from the mixer are shifted out of the base band. The resulted beat note spectrum is shown in Fig. 10 (a), plotted against the offset frequency from 543 kHz. Also plotted is the same beat signal without atmospheric transmission, realized by diverting the pulse train in the transmission arm through a fiber link of about 40 m long. The fiber is cut in such a way that it produces the same amount of time delay as the 60-m atmospheric link. Such an arrangement allows us to assess the contribution of the laser and the amplifier in our phase noise measurement.

Due to the imbalance of the interferometer, amplitude and phase noise from the laser and the EDFA could enter the heterodyne signal. One particular concern is that, because of the free-running laser, the drift of the laser repetition rate and carrier-envelope offset frequency may also broaden the beat note. With the fiber link, transmission-induced excess phase noise is much smaller (Holman et al., 2004), allowing us to assess the upper limit of the noise contribution from the laser and the amplifier. In Fig. 10 (a), both traces have a resolution bandwidth of 16 Hz, and are averaged over 1 s. The resolution limited sharp peak in the spectrum from fiber transmission indicates that the femtosecond laser and the EDFA has a negligible effect in the current excess phase noise characterization. In comparison, the atmospheric transmission causes significant spectral broadening. The broadened beat note spectrum has a full width of approximately 1 kHz.

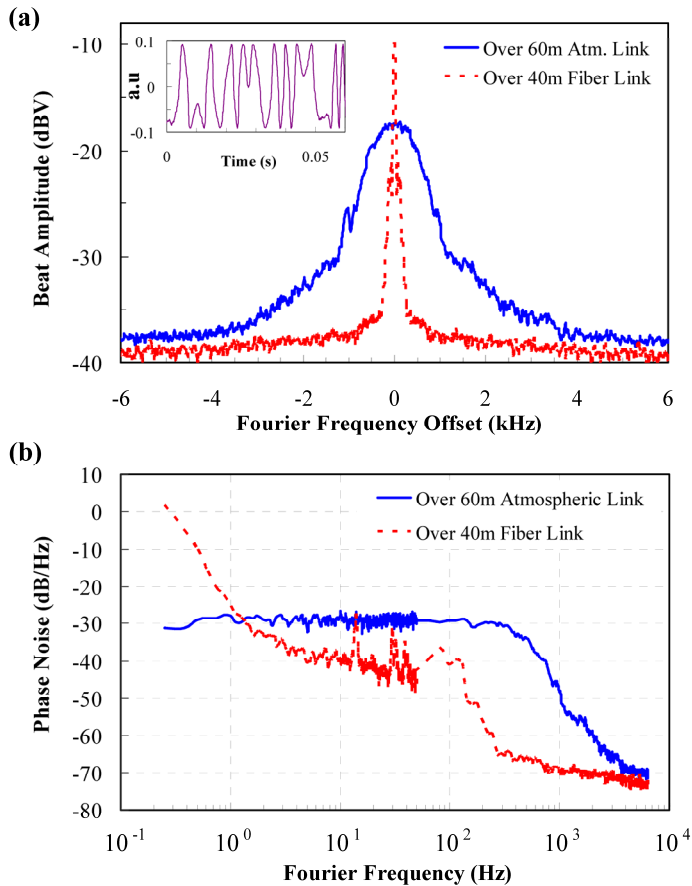


Fig. 10. (a) Fourier spectra of the 543-kHz heterodyne beat note for 60-m atmospheric transfer (solid) and 40-m fiber optic transfer (dashed). Significant linewidth broadening (\sim kHz) is caused by the atmospheric propagation in comparison with fiber transmission. Inset: A time-domain trace of the homodyne beat note for atmospheric transfer demonstrates the large phase fluctuation. (b) Phase noise spectra of the 543-kHz beat note with the above two transfer cases.

A close look at the noise characteristics of the two transmission cases near the nominal frequency can be gained through their phase noise spectra, which are assembled from data over two frequency spans and are shown in Fig. 10 (b). It has been shown that such heterodyne phase noise can be understood as the zeroth-order excess phase noise of all the comb lines (Gollapalli & Duan, 2011). Since the beat note from the atmospheric transmission has no coherent spike as the carrier, the two curves in Fig. 10 (b) are normalized to their total signal powers (i.e., the integration of the beat note spectra) instead of the carrier power. A frequency-independent noise spectrum is seen below 300 Hz for the beat note from the atmospheric transmission. It is followed by a quick roll-off above 500 Hz. Such characteristics seem to agree with the spectral features for a slow phase modulation with a

very large modulation index. In comparison, transmission in fibre with the same time delay results in a much smaller phase noise. The spikes between 10–100 Hz are believed to be the result of acoustic noise and electronic interference from the power circuits inside the lab. The above comparison shows that atmospheric fluctuations add a significant amount of phase noise to the optical frequency references transmitted through the air. As a result, atmospheric transfer of optical frequencies in general suffers much larger short-term fluctuations when compared with fibre-optic transfer.

For many applications, however, a more relevant parameter is the long-term stability of the frequency transfer scheme, which can be evaluated by measuring the Allan deviation of the 543-kHz beat note. Shown in Fig. 11 (a) are several sets of measured data of the Allan deviation versus the averaging time through the 60-m transmission link under various

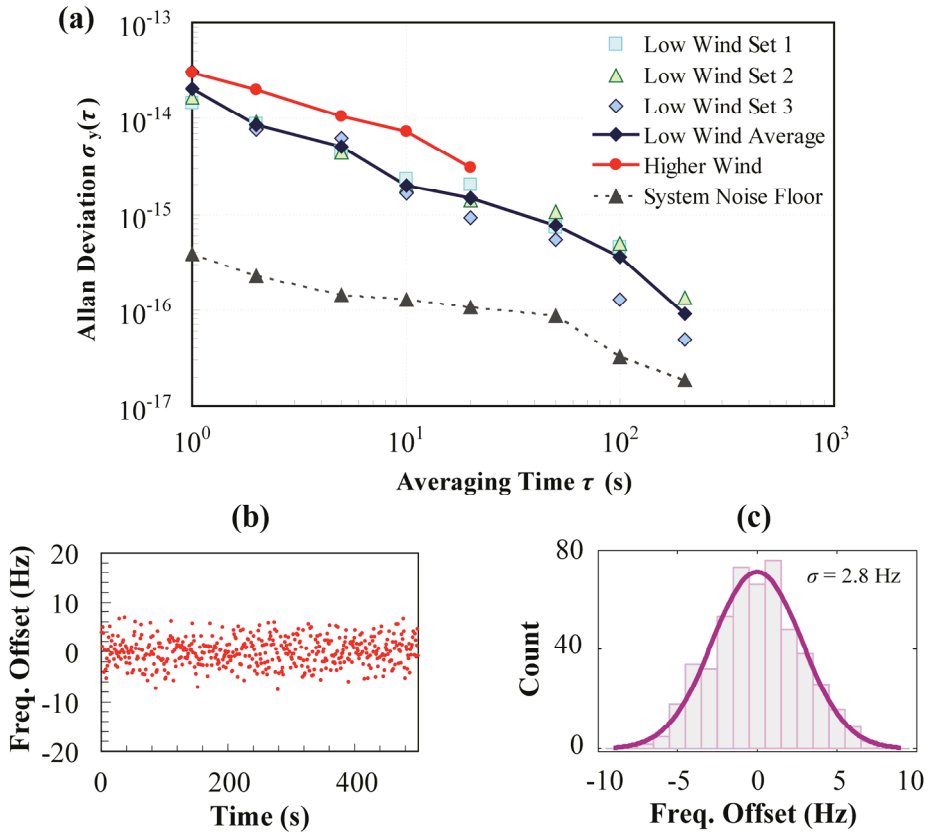


Fig. 11. (a) Allan deviations of the 543-kHz heterodyne beat note for 60-m atmospheric transfer under various weather conditions and the system noise floor. (b) A data set of 500 consecutive frequency measurements at 1-s gate time, plotted relative to the nominal frequency. (c) The histogram of (b), overlaid with a fitting to the normal distribution, leads to a standard deviation of 2.8 Hz for the frequency references transferred across the atmospheric link.

weather conditions. Among them, three sets were taken under low-wind conditions, with the wind speed generally staying below 5 mph (miles-per-hour), or 2.2 m/s, throughout the data collection periods (except for Set #1 at 200 s, which is not included here). The average of these data shows an overall behaviour of the Allan deviation close to τ^{-1} within the measurement range. The fractional frequency stability at 1 s is about 2×10^{-14} . When averaged over 100 s, the stability improves to 10^{-16} level. Over even longer time, however, the beat note often develops large power fluctuation, which prevents a reliable measurement of the Allan deviation with an averaging time longer than 200 s. The fluctuation of the beat note power is believed to be caused by the transmitted and the reference pulses drifting away from their optimum overlapping position due to the change of the effective path length of the transmission link. To demonstrate the effect of wind, we also include here a set of data taken under stronger wind, with wind speed ranging between 7–14 mph over the data collection period. Below 20 s, the higher-wind data stay roughly 3 dB above the average low-wind data and display a similar τ^{-1} dependence. No Allan deviation was successfully measured above 20 s due to the power fluctuation of the beat note. In addition, a set of baseline data is also included in Fig. 11 (a) to mark the system-limited measurement resolution. It is obtained by reflecting the transmission beam immediately into the receiving subsystem so the length of atmospheric propagation is negligible.

To further verify the scale of the frequency fluctuation, we take a close look at the measured beat note frequencies. Fig. 11 (b) shows consecutive readings of the frequency counter over several minutes with a 1-s gate time, taken under the low-wind condition. The frequencies have been offset to the nominal value of 543 kHz. A histogram analysis shows that the frequencies have a normal distribution around the nominal frequency, as shown in Fig. 11 (c), and a Gaussian fitting results in a standard deviation of 2.8 Hz. This frequency fluctuation level is in agreement with the Allan deviation measurement for low wind.

5.3 Discussion

To put our work into context, it is interesting to compare the above results with some of the previous reports on optical frequency transfer in the atmosphere. Sprenger et al. made a similar rooftop demonstration using a cw diode laser over a 100-m atmospheric link at the ground level (Sprenger et al., 2009). The group achieved an Allan deviation of 2×10^{-13} at 1 s. In addition, a statistics of the beat note frequency measured with a 1-s gate time shows a 70.5-Hz full width at half maximum. Compared with this work, the current study reports a frequency instability one order of magnitude lower at 1 s. Apart from the apparent shorter transmission distance, the smaller frequency fluctuation in the current work is likely due to the low-wind condition (< 2 m/s), which means lower index fluctuation due to air turbulence. Such a fact is evident in Fig. 11 (b), where continuous frequency measurement over several minutes shows a consistently low frequency fluctuation. More recently, Djerroud et al. have reported a coherent optical link across 5 km of turbulent atmosphere based on a cw Nd:YAG laser (Djerroud et al., 2010). A remarkably low Allan deviation of 1.3×10^{-14} is achieved at 1 s, and the stability further improves to 2×10^{-15} at 100 s. The authors, however, did point out that the experiment took place at an observatory 1323 m above the sea level, which could account, at least in part, for the high degree of frequency stability

over a long distance. Based on the standard Kolmogorov model of atmospheric turbulence, the power spectral density of index fluctuation, Φ_n , is given by $\Phi_n(\kappa) = 0.033C_n^2\kappa^{-11/3}$, where C_n is the index structure constant and κ is the spatial wave number. Experimentally, it has been shown that C_n strongly depends on altitude (Ishimaru, 1978). For example, the altitude of Huntsville is 200 m, which corresponds to a C_n of approximately $10^{-7} \text{ m}^{-1/3}$ for sunny days. At 1323 m, however, C_n is about $10^{-8} \text{ m}^{-1/3}$ under similar conditions, which indicates a refractive index fluctuation roughly two orders of magnitude smaller than it at 200 m altitude.

6. Summary

In summary, we have experimentally demonstrated the transfer of clock signals in both microwave and optical frequency ranges over an open atmospheric transmission link using a femtosecond frequency comb. The excess phase noise due to the atmospheric propagation is successfully characterized in both cases, and the both results show large, slow-frequency phase modulations due to the index fluctuation of air. The fractional frequency stability for a 60-m transmission under typical calm weather conditions is in the order of a few parts per 10^{12} for microwave clock transfer and a few parts per 10^{14} for optical clock transfer, both with a 1-s averaging time. The much better fractional stability for optical clock transfer is mainly attributed to the much higher clock frequencies, which demonstrates the advantage of shifting reference clocks toward higher frequencies. Our measurement also shows an approximate τ^{-1} dependence of the Allan deviation on the averaging time in both frequency ranges up to 200 s. This is an encouraging finding for atmospheric clock transfer because it means that, over longer time, transferring a highly stable master clock via free space can be more advantageous than maintaining a less-precise local clock, which normally has a $\tau^{-1/2}$ dependence. Further study under more diverse weather conditions and over longer transmission distances is needed to confirm this results.

Two key properties of photodetectors play critical roles in the current research. The square-law detector allows us to perform optical heterodyne to characterize the excess phase noise in optical frequency transfer. Meanwhile, power-to-phase coupling in photodetectors puts a requirement on the receiving optics to keep the impact of beam wander and speckle low.

Further improvement of the clock transfer stability would require the use of active noise cancellation. Such a scheme has been demonstrated to be able to lower the transfer-induced instability by a factor of 10 in fiber-optic systems (Holman et al., 2005). To apply a similar technique in free space, retroreflection is needed to allow the returning beam to travel exactly the same path back in order to avoid differences in phase noise caused by different paths. In addition, the locking system likely needs to have a much wider bandwidth compared to the fiber-optic scheme even for a moderate transmission distance (e.g. 100 m) because of the relatively fast turbulence-induced index fluctuation in the air.

7. Acknowledgment

We would like to acknowledge Mr. Ted Rogers and Dr. Robert Lindquist of the Center for Applied Optics, the University of Alabama in Huntsville, for their assistance in the setup of

the atmospheric transmission link. Ms Ayshah Alatawi made key contributions to the lab test of the microwave clock transfer. The work was supported in part by grants from UAH.

8. References

- Akozbeq, N.; Bowden, C. M.; Talebpour, A. & Chin, S. L. (2000). Femtosecond pulse propagation in air: Variational analysis, *Physics Review E*, Vol.61, pp. 4540-4549
- Alatawi, A.; Gollapalli, R. P. & Duan, L. (2009). Radio frequency clock delivery via free-space frequency comb transmission, *Opt. Lett.*, Vol.34, pp. 3346-3348
- Allan, D. W. (1966). Statistics of atomic frequency standards, *Proc. IEEE*, Vol.54, pp. 221-230
- Altarelli, M (eds) et al. (2007). XFEL: The European X-Ray Free Electron Laser, *Technical Design Report DESY 2006-097* (DESY, Hamburg, 2007), at <http://xfel.desy.de>
- Andrews, L. C. & Phillips, R. L. (2005). *Laser beam propagation through random media*, SPIE Press, 2nd Ed.
- Bartels, A.; Oates, C. W.; Hollberg, L. & Diddams, S. A. (2004). Stabilization of femtosecond laser frequency combs with subhertz residual linewidths, *Optics Letters*, Vol.29, pp. 1081-1083
- Bartels, A.; Diddams, S. A.; Oates, C. W.; Wilpers, G.; Bergquist, J. C.; Oskay, W. H. & Hollberg, L. (2005). Femtosecond-laser-based synthesis of ultrastable microwave signals from optical frequency references, *Optics Letters*, Vol.30, pp. 667-669
- Brookner, E. (1970). Atmosphere propagation and communication channel model for laser wavelengths, *IEEE Trans. Commun. Technol.*, COM-18, pp. 396-416
- Chan, V. W. S. (2006). Free-space optical communications, *J. Lightwave. Technol.* Vol.24, pp. 4750-4762
- Ciddor, P. E. (1996). Refractive index of air: new equations for the visible and near infrared, *Appl. Opt.*, Vol. 35, pp. 1566-1573
- Ciddor P. E. and Hill, R. J. (1999). Refractive index of air. 2. group index, *Appl. Opt.*, Vol.38, pp. 1663-1667
- Cliche, J. F. & Shillue, B. (2006). Precision timing control for radioastronomy, *IEEE Control Sys. Mag.* Vol.26, pp. 19-26
- Davis, C. C. 1996. *Lasers and Electro-Optics Fundamentals and Engineering*, Cambridge University Press
- Djerroud, K.; Acef, O.; Clairon, A.; Lemonde, P.; Mar, C. N.; Samain, E. & Wolf, P. (2010). Coherent optical link through the turbulent atmosphere, *Opt. Lett.*, Vol.35, pp. 1479-1481
- Foreman, S. M.; Holman, K. W.; Hudson, D. D.; Jones, D. J. & Ye, J. (2007). Remote transfer of ultrastable frequency references via fibre networks, *Review of Scientific Instruments*, Vol.78, pp. 021101
- Fortier, T. M.; Le Coq, Y.; Stalnaker, J. E.; Ortega, D.; Diddams, S. A.; Oates, C. W. & Hollberg, L. (2006). Kilohertz-resolution spectroscopy of cold atoms with an optical frequency comb, *Physical Review Letters*, Vol.97, pp. 163905
- Gollapalli, R. P. & Duan, L. (2010). Atmospheric timing transfer using a femtosecond frequency comb, *IEEE Photon. Journal*, Vol.2, pp. 904-910
- Gollapalli, R. P. & Duan, L. (2011). Multiheterodyne Characterization of Excess Phase Noise in Atmospheric Transfer of a Femtosecond-Laser Frequency Comb, *Journal of Lightwave technology*, Vol.29, pp. 3401-3407.

- Halford, D.; Wainwright, A. E. & Barnes, J. A. (1968). Flicker noise of phase in RF amplifiers and frequency multipliers: characterization, cause, and cure, *22nd Annual Symposium on Frequency Control*, pp. 340.
- Hall, J. L. & Ye, J. (2003). Optical frequency standards and measurement, *IEEE Trans. Instrum. Meas.*, Vol.52, pp. 227-230
- Holman, K. W.; Jones, D. J.; Hudson, D. D. & Ye, J. (2004). Precise frequency transfer through a fiber network by use of 1.5 μ m mode-locked sources, *Optics Letters*, Vol.29, pp. 1554-1556
- Holman, K. W.; Hudson, D. D., Ye, J. & Jones, D. J. (2005). Remote transfer of a high-stability and ultralow-jitter timing signal, *Optics Letters*, Vol.30, pp. 1225-1227
- Holzwarth, R.; Udem, T.; Hansch, T. W.; Knight, J. C.; Wadsworth, W. J. & Russell, P. St. J. (2000). Optical frequency synthesizer for precision spectroscopy, *Physical Review Letters*, Vol.85, pp. 2264-2267
- Hong, S. T.; Sreenivasiah, I. & Ishimaru, A. (1977). Plane wave pulse propagation through random media, *IEEE Transactions on Antennas and Propagation*, AP-25, pp. 822-828
- IEEE Std. 1139-1988, IEEE standard definitions of physical quantities for fundamental frequency and time metrology (IEEE, 1983).
- Ishimaru, A. 1978. *Wave Propagation and Scattering in Random Media*, Academic, New York
- Ivanov, E. N.; Diddams, S. A. & Hollberg, L. (2003). Analysis of noise mechanisms limiting the frequency stability of microwave signals generated with a femtosecond laser, *IEEE J. Select. Topics Quantum Electron*, Vol.9, pp. 1059-1065
- Jones, D. J.; Diddams, S. A.; Ranka, J. K.; Stentz, A.; Windeler, R. S.; Hall, J. L. & Cundiff, S. T. (2000). Carrier-envelope phase control of femtosecond mode-locked lasers and direct optical frequency synthesis, *Science*, Vol.288, pp. 635-639
- Kim, J.; Cox, J. A.; Chen, J. & Kaertner, F. X. (2008). Drift-free femtosecond timing synchronization of remote optical and microwave sources, *Nature Photonics*, Vol.2, pp. 733-736
- Li, C. H. et al. (2008). A laser frequency comb that enables radial velocity measurements with a precision of 1 cm/s¹, *Nature*, Vol.452, pp. 610-612,
- Liu, C. H.; Wernik, A. W. & Yeh, K. C. (1974). Propagation of pulse trains through a random medium, *IEEE Transactions on Antennas and Propagation*, Vol.22, pp. 624-627
- Liu, P. L.; Williams, K. J.; Frankel, M. Y. & Esman, R. D. (1999). Saturation characteristics of fast photodetectors, *IEEE Trans. Microwave Theory Tech*, Vol.47, pp. 1297-1303
- Mlejnek, M.; Kolesik, M.; Moloney, J. V. & Wright, E. M. (1999). Optically turbulent femtosecond light guide in air, *Physics Review Letters*, Vol.83, pp. 2938-2941
- Nahin, P. J. 2001. *The Science of Radio*, AIP Press, New York: Springer-Verlag
- Prucnal, P.; Santoro, M. & Sehgal, S. (1986). Ultrafast All-Optical Synchronous Multiple Access Fiber Networks, *Selected Areas in Communications*, Vol.4, pp. 1484-1493
- Ricklin, J. C. & Davidson, F. M. (2003). Atmospheric optical communication with a Gaussian Shell beam. *J. Opt. Soc. Am. A*, Vol.20, pp. 856-866
- Rodriguez, M.; Bourayou, R.; Mejean, G.; Kasparian, J.; Yu, J.; Salmon, E.; Scholz, A.; Stecklum, B.; Eisloffel, J.; Laux, U.; Hatzes, A. P.; Sauerbrey, R.; Woste, L. & Wolf, J. (2004). Kilometer-range nonlinear propagation of femtosecond laser pulses, *Physics Review E*, Vol.69, pp. 036607
- Rutman, J. & Walls, F. (1991). Characterization of frequency stability in precision frequency sources, *Proc. IEEE*, Vol.79, pp. 952-960

- Shaik, K. S. (1988). Atmospheric propagation effects relevant to optical communications, *TDA Progress Report*, pp. 42-94
- Sprangle, P.; Penano, J. R. & Hafizi, B. (2002). Propagation of intense short laser pulses in the atmosphere, *Physics Review E*, Vol.66, pp. 046418
- Sprenger, B. ; Zhang, J.; Lu, Z. H. & Wang, L. J. (2009). Atmospheric transfer of optical and radio frequency clock signals, *Opt. Lett.*, Vol.34, pp. 965-967
- Su, H. H. & Plonus, M. A. (1971). Optical-pulse propagation in a turbulent medium, *J. Opt. Soc. Am.* Vol.61, pp. 256-260
- Thorpe, M. J.; Moll, K. D.; Jones, R. J.; Safdi, B. & Ye, J. (2006). Broadband cavity ringdown spectroscopy for sensitive and rapid molecular detection, *Science*, Vol.311, pp. 1595-1599
- Tulchinsky, D. A. & Williams, K. J. (2005). Excess amplitude and excess phase noise of RF photodiodes operated in compression, *IEEE Photonics Technology Letters*, Vol.17, pp. 654-656
- Udem, Th.; Diddams, S. A.; Vogel, K. R.; Oates, C.W.; Curtis, E. A.; Lee, W. D.; Itano, W. M.;Drullinger, R. E.; Bergquist, J.C. & Hollberg, L. (2001). Absolute frequency measurements of the Hg and Ca optical clock transitions with a femtosecond laser, *Physical Review Letters*, Vol.86, pp. 4996-4999
- Udem, T.; Holzwarth, R. & Hansch, T. W. (2002). Optical frequency metrology, *Nature*, Vol.416, pp. 233-237
- Ye, J. (2004). Absolute measurement of a long, arbitrary distance to less than an optical fringe, *Optics Letters*, Vol.29, pp. 1153-1155
- Young, C. Y.; Andrews, L. C. & Ishimaru, A. (1998). Time-of-arrival fluctuations of a space-time Gaussian pulse in weak optical turbulence: An analytic solution, *Applied Optics*, Vol.37, pp. 7655-7660